Computational study on band structure engineering using graphene nanomeshes

Sako, Ryutaro
Hasegawa, Naomi
Tsuchiya, Hideaki
Ogawa, Matsuto

(Citation)
Journal of Applied Physics,113(14):143702-143702

(Issue Date)
2013-04-14

(Resource Type)
journal article

(Version)
Version of Record

AIP Journal of Applied Physics

Computational study on band structure engineering using graphene nanomeshes

Ryūtaro Sako, Naomi Hasegawa, Hideaki Tsuchiya, and Matsuto Ogawa

Citation: Journal of Applied Physics **113**, 143702 (2013); doi: 10.1063/1.4800624
View online: http://dx.doi.org/10.1063/1.4800624
View Table of Contents: http://scitation.aip.org/content/aip/journal/jap/113/14?ver=pdfcov
Published by the AIP Publishing

Computational study on band structure engineering using graphene nanomeshes

Ryūtaro Sako,[1] Naomi Hasegawa,[1] Hideaki Tsuchiya,[1,2,a)] and Matsuto Ogawa[1]
[1]*Department of Electrical and Electronic Engineering, Graduate School of Engineering, Kobe University, 1-1, Rokko-dai, Nada-ku, Kobe 657-8501, Japan*
[2]*Japan Science and Technology Agency, CREST, Chiyoda, Tokyo 102-0076, Japan*

(Received 26 November 2012; accepted 25 March 2013; published online 8 April 2013)

Graphene nanomeshes (GNMs) are expected to be a high-performance channel material for metal-oxide-semiconductor field-effect-transistors (MOSFETs), since they can open up a band gap in a large sheet of graphene thin film by simply introducing two-dimensional periodical nanoscale holes. In this paper, we theoretically investigate the electronic band structures and the electron transport properties of GNMs based on a tight-binding approach. We demonstrate that GNMs have the capability of band structure engineering by controlling its neck width and furthermore the potential ability providing high current drivability when applied to a field-effect-transistor channel.
 [http://dx.doi.org/10.1063/1.4800624]

I. INTRODUCTION

Graphene has significant potential for application in field-effect-transistor (FET) channel, because it has very high carrier mobility as compared to Si and other semiconductor materials.[1] However, it is a semimetal with a zero band gap, and thus it cannot be used as a switching device in logic circuits, which requires a large on/off current ratio. Therefore, opening a finite band gap in a semimetal graphene is one of the most important subjects in graphene research. One of the techniques is to use bilayer graphene (BLG) applied by a vertical electric field.[2–7] Although BLG can be fabricated using a large-area graphene sheet, stacking only two layers uniformly in a large-area is still difficult using the current technologies. In addition, the band gap of BLG has been reported to be saturated at $0.2 \sim 0.3$ eV[3,8,9] and has negative effective masses at K and K' points,[3,4,8,10,11] called Mexican-hat structure. The other technique is to pattern a graphene sheet into a nanoribbon having widths of less than 10 nm,[12–17] which is named graphene nanoribbon (GNR). The band gap of GNR is generated by quantum confinement effect and increases inversely with the ribbon width. Theoretical calculations[13,16,18–20] have reported that GNR exhibits band gaps larger than those of BLG and no Mexican-hat structure. Therefore, GNR is attractive for a FET channel material, but its electron transport properties are extremely sensitive to ribbon edge configuration, that is, zigzag-edged or armchair-edged configuration. In general, a zigzag-edged GNR (Z-GNR) has localized states at the edges and nearly zero-band gap, while an armchair-edged GNR (A-GNR) exhibits a large band gap and a small transport effective mass. Accordingly, A-GNR is considered to be suitable for the FET application.[13] However, the fabrication of pure A-GNR channels with a certain amount of length and the production of dense arrays of ordered nanoribbons still remains a significant challenge, and then drastic degradation in the device performance due to atomic fluctuation of the ribbon width and the edge conformation has been pointed out.[21–24]

Recently, a new graphene nanostructure for opening a finite band gap, which is called graphene nanomesh (GNM), has been reported.[25,26] GNM is composed of single-layer graphene into which a high-density array of nanoscale holes are punched, and can open up a band gap, comparable with the values achieved in GNRs, in a large sheet of graphene thin film. Actually, it was demonstrated that GNM-FETs provide driving currents nearly 100 times greater than individual GNR-FETs, and the on-off current ratio, that is, the band gap opening can be tuned by varying the neck width.[25,26] GNM lattices are also considered to be much easier to produce and handle than GNRs. These features indeed make GNM attractive for a FET channel material. However, since the nanomeshes have variable periodicities, neck widths, shapes of nanohole, edge configurations, and so on, their electric properties indicate quite complicated behaviors. So far, circular nanoholes[27,28] or triangular/rhombus nanoholes with an armchair-edge or a zigzag-edge structure[29] have been discussed. In this study, to clarify the roles of the edge configuration in GNMs, we investigate the electron transport properties in GNMs with rectangular-shaped nanoholes combined with armchair-edged and zigzag-edged nanoribbons. We calculate the band structures by varying the neck width based on a tight-binding (TB) approach, and then estimate the electrical characteristics of GNM-FETs under the ballistic transport. We demonstrate the possibility of band structure engineering by controlling the neck width, and the potential ability of GNM-FET achieving high current drivability.

II. BAND STRUCTURES OF GNMS

To clarify the roles of the edge configuration, we adopted a rectangular-shaped nanohole as shown in Fig. 1, where h_x and h_y denote the numbers of carbon atoms of a nanohole in x- and y-directions, respectively. As seen in

a)Author to whom correspondence should be addressed. Electronic mail: tsuchiya@eedept.kobe-u.ac.jp. Tel./Fax: +81-78-803-6082.

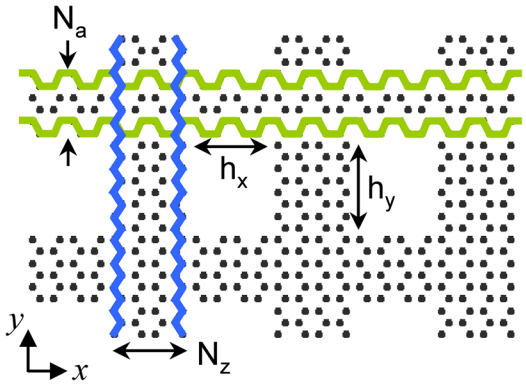

FIG. 1. Atomic model of GNM used in the simulation. The horizontal and vertical sides of nanoholes have an armchair-edged and zigzag-edged configuration, respectively.

Fig. 1, the horizontal and vertical sides of nanoholes have an armchair-edged and zigzag-edged configuration, respectively. Therefore, we expect to be able to control a contribution from the A-GNRs, which have superior transport properties as mentioned above, by changing the corresponding neck width. To this end, we fixed the number of carbon atoms in the zigzag-edged neck, N_z, and varied that in the armchair-edged neck, N_a, and then computed the band structures based on TB approach using a p_z orbital basis set.[30] The TB parameters used in the calculation are the same as in Refs. 8, 9, and 20. Here, we add that the armchair-edged neck in the present calculation is composed of $N_a = 3m$ group (m is a positive integer), because it is expected to demonstrate superior transport properties over $N_a = 3m+1$ and $3m+2$ groups.[20] Edge bond relaxation introduced in A-GNR calculations[16,18,20,31] is not taken into account, because there is no detailed information for GNMs yet.

First, we present the computed band structures for GNMs with $N_a = 3$, 6, 9, 12, and 15 in Figs. 2 and 3, where N_z is fixed to be 4 and 8, respectively. The inset in Fig. 2(a) represents the first Brillouin zone with the three high-symmetry axes indicated, along which the band structure was calculated. The atomic models used in the calculation are also plotted with the unit cells. The energy reference in the vertical axis ($E = 0$) represents the Fermi energy, and thus the positive and negative energy regions correspond to conduction and valence bands, respectively. First of all, it is found that the band gap is larger for an odd-numbered N_a, i.e., $N_a = 3$, 9, and 15 for both N_z's. Furthermore, the dispersion curves at the conduction band minimum exhibit quite different behavior between odd-numbered and even-numbered N_a's. In other words, the flat dispersion curves, marked with Z in $N_a = 3$, 9, and 15, are nearly dispersionless along the Γ-X direction and their energies hardly change with increasing N_a. In addition, the concave dispersion curves, marked with A, decrease in energy with increasing N_a. On the other hand, the lowest conduction bands, marked with A' in $N_a = 6$ and 12, exhibit a concave dispersion around the Γ point, and then changes into a flat dispersion with increasing the energy. Furthermore, the band A' have a smaller band gap opening at the Γ point. From these characteristic behaviors, we speculated that the band A and band Z originated mainly from the A-GNR neck and the Z-GNR neck, respectively, while the band A' originated from both GNR necks. Similar behaviors at the conduction band

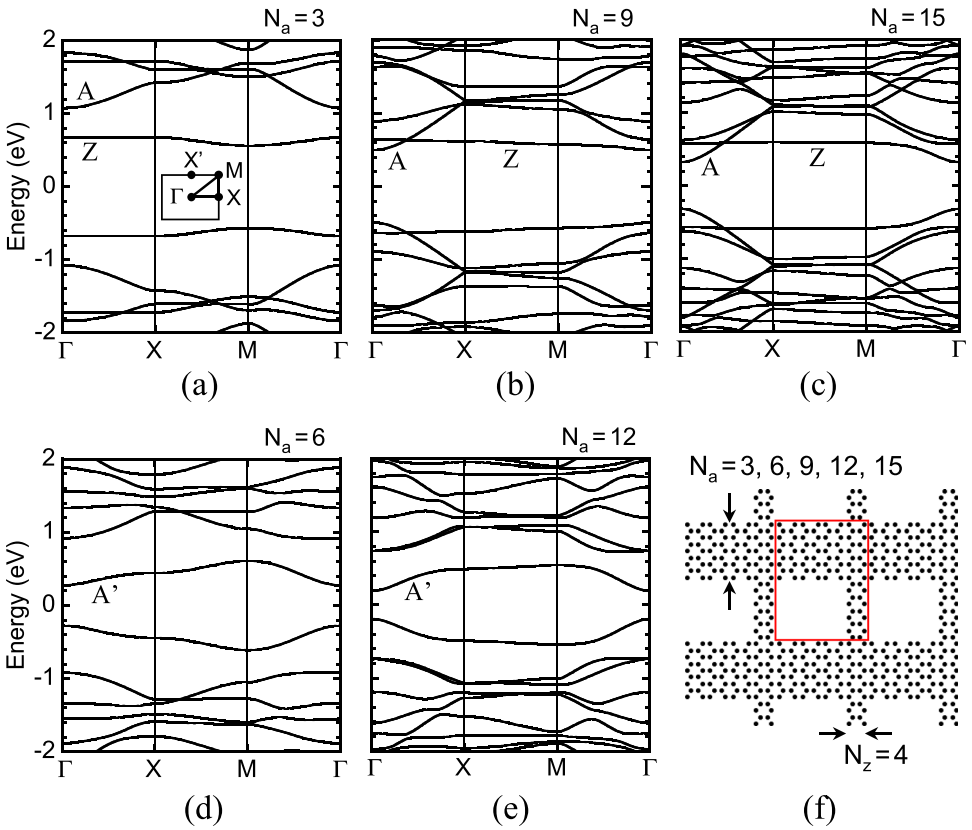

FIG. 2. Computed band structures for GNMs with N_a = (a) 3, (b) 9, (c) 15, (d) 6, and (e) 12, where N_z is fixed to be 4. (h_x, h_y) = (12, 9) in (a), (b), and (c), and (12, 8) in (d) and (e). The atomic model used in the calculation is plotted with the unit cell in (f). The inset in (a) represents the first Brillouin zone with the three high-symmetry axes indicated, along which the band structure was calculated.

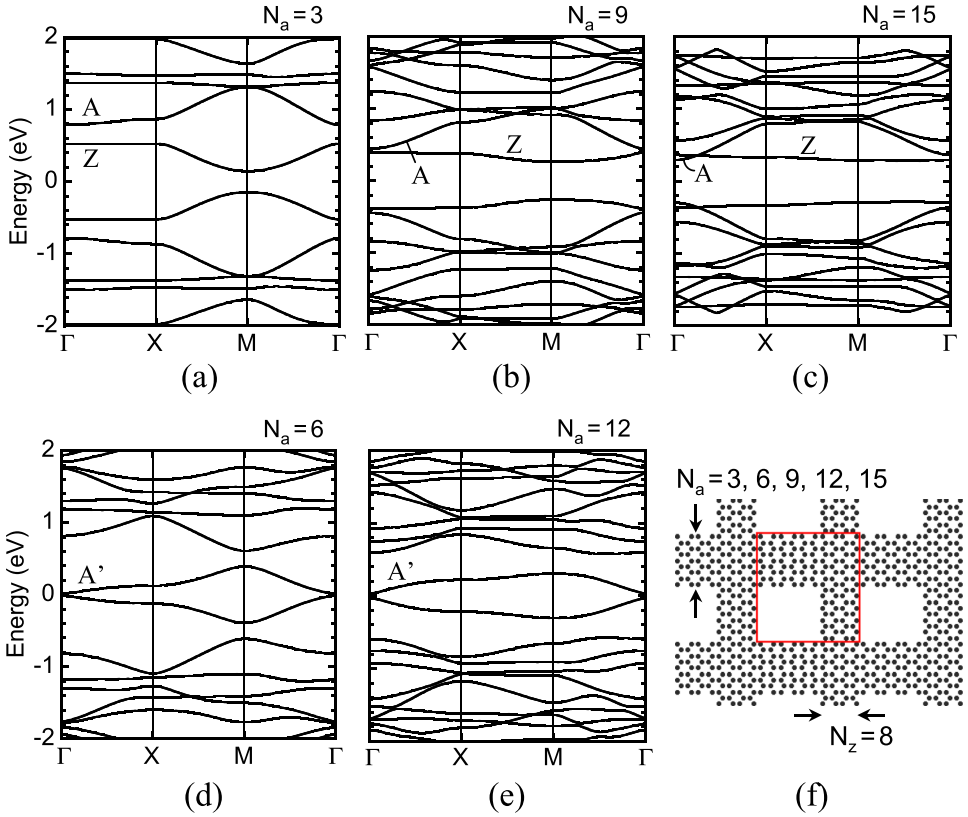

FIG. 3. Computed band structures for GNMs with N_a = (a) 3, (b) 9, (c) 15, (d) 6, and (e) 12, where N_z is fixed to be 8. (h_x, h_y) is the same as in Fig. 2. (f) The atomic model used in the calculation with the unit cell.

minimum have also been reported for armchair-edged triangular and rhombus graphene nanoholes[29] and circular graphene nanoholes.[27,28] Thus, our band structure results are applicable to estimate the electrical characteristics of GNM-FETs.

To confirm the validity of the above speculation, we calculated the probability density distributions of electrons at the Γ point for $N_a = 9$ and 12 with $N_z = 4$ as shown in Fig. 4, where (a) the band A and band Z in $N_a = 9$ and (b) the band A' in $N_a = 12$. The distributions only inside the unit cells are plotted. It should be noted that the band A in $N_a = 9$ has nearly localized density distribution in the A-GNR neck, while the band Z is strongly localized in the Z-GNR neck. These spatially separated density distributions prove that the band A and band Z originated mainly from the A-GNR neck and the Z-GNR neck, respectively. In Fig. 4, we also plotted the conduction band structures along k_x and k_y directions, which correspond to the Γ-X and Γ-X' directions in Fig. 2, respectively. Since electrons in the band A are unable to travel freely across the Z-GNRs in the y-direction, the dispersion in the k_y direction is found to be rather flat as compared to the band A in the k_x direction. In addition, an energy minimum appears at the X' point. Such an anisotropic behavior has also been discussed for graphene under periodic potentials.[32] Understandably, a higher current is expected to be obtained in the x-direction having the armchair-edged structure. On the other hand, for the band A' in $N_a = 12$, electrons are distributed in the whole region as shown in Fig. 4(b), in other words, they are not localized in any particular region, and hence the band A' has a normal concave dispersion also in the k_y direction. However, an anisotropic behavior is observed even in the present case. The above results indicate that the band A' receives influences from both GNR necks.

Next, we checked the N_a dependences of the band gap and effective mass at the Γ point of the band A and A' as

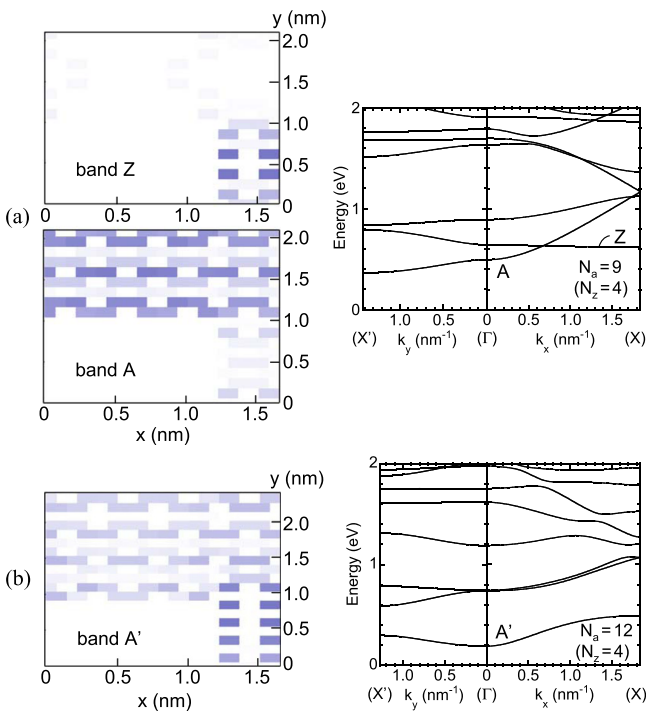

FIG. 4. Probability density distributions of electrons at Γ point computed for $N_a = 9$ and 12 with $N_z = 4$, where (a) the band A and band Z in $N_a = 9$ and (b) the band A' in $N_a = 12$. The distributions only inside the unit cells are plotted. Conduction band structures along k_x and k_y directions, which correspond to the Γ-X and Γ-X' directions in Fig. 2, respectively, are also plotted.

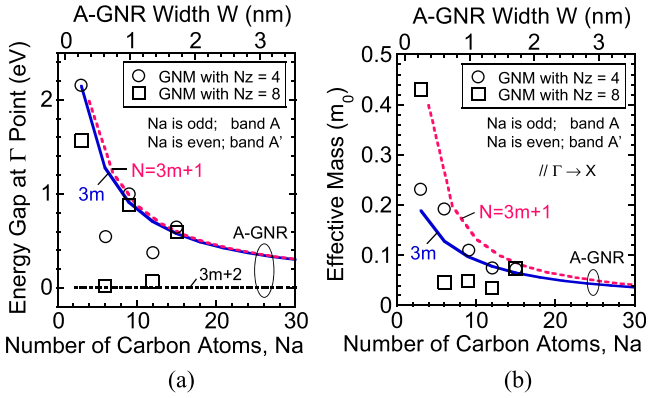

FIG. 5. (a) Band gaps and (b) effective masses at Γ point of band A and A', computed as a function of N_a. Here, the calculated results for pure A-GNRs without edge bond relaxation are also plotted in the lines.

shown in Fig. 5, where the results calculated for pure A-GNRs without edge bond relaxation[20] are also plotted for comparison. As for the band gap, GNMs with odd-numbered N_a's, i.e., the band A, closely follow the curve for the $N_a = 3m$ group of pure A-GNRs, which confirms that the band A is surely derived from the A-GNR neck. On the other hand, the effective masses of GNMs with $N_z = 8$ stray far from the curve for the $N_a = 3m$ group, which is considered due to an influence of coupling with a Z-GNR band, but the details are still under consideration. As for $N_z = 4$, the effective mass monotonically decreases with N_a, in keeping with the curve for the $N_a = 3m$ group. Consequently, GNMs with an odd-numbered N_a and a fewer N_z are considered to be suitable to assess the upper limit performance of GNM-FETs, since the superior transport properties of A-GNR can be exploited. Then, we will examine the electrical characteristics of GNM-FETs with $N_a = 3$, 9, and 15 and $N_z = 4$, in Sec. III.

III. ELECTRICAL CHARACTERISTICS OF GNM-FETS UNDER BALLISTIC TRANSPORT

In this study, we employed a top-of-the-barrier (ToB) FET model[33] as shown in Fig. 6, where the source-drain direction is set along the x-axis which has the armchair-edged structure,

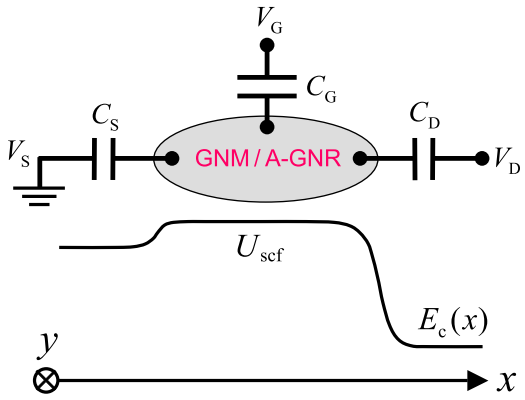

FIG. 6. ToB ballistic FET model used in the simulation. We assumed that the gate has perfect electrostatic control over the channel and that the source and drain are heavily doped contacts with $N_D = 3.35 \times 10^{16}$ m^{-2} and the channel is undoped. The gate insulator is SiO_2 and its thickness T_{ox} is given as 1.5 and 0.5 nm.

and a higher current drivability is expected. The ToB model is simple but is very helpful to understand the importance of atomistic band structures in the metal-oxide-semiconductor FETs (MOSFETs). Since source-drain direct tunneling and scattering effects are not considered, it will provide the upper limit performance of atomistic transistors.[13,33] We assumed that the gate has perfect electrostatic control over the channel, and that the source and drain are heavily doped contacts with $N_D = 3.35 \times 10^{16}$ m^{-2} and the channel is undoped. The gate insulator is SiO_2 and its thickness T_{ox} is given as 1.5 and 0.5 nm. The drain voltage V_D is set at 0.3 V, which is sufficiently small so that band-to-band tunneling leakage current can be neglected. Fig. 7 shows the electrical characteristics computed for the GNM-FETs with $N_a = 3$ (dotted lines), 9 (dashed lines), and 15 (solid lines) for T_{ox} = (a) 1.5 and (b) 0.5 nm, where N_z was fixed to be 4. The drain current I_D, the sheet electron density n and the average electron velocity $\langle v \rangle$ as a function of gate voltage are indicated beginning at the top. The OFF-current density is all set as 0.01 μA/μm. First of all, the GNM with $N_a = 3$ indicates the considerably inferior performance due to the involvement from the nearly dispersionless band Z as shown in Fig. 2(a). Next, the drain current of $N_a = 15$ is larger than that of $N_a = 9$ for both T_{ox}'s. This is because the GNM with $N_a = 15$ has the higher average velocity and the almost equal sheet density, as compared with those of $N_a = 9$. The higher average velocity in $N_a = 15$ is due to the smaller effective mass and also due to the larger energy separation from the upper conduction band with a flat dispersion.

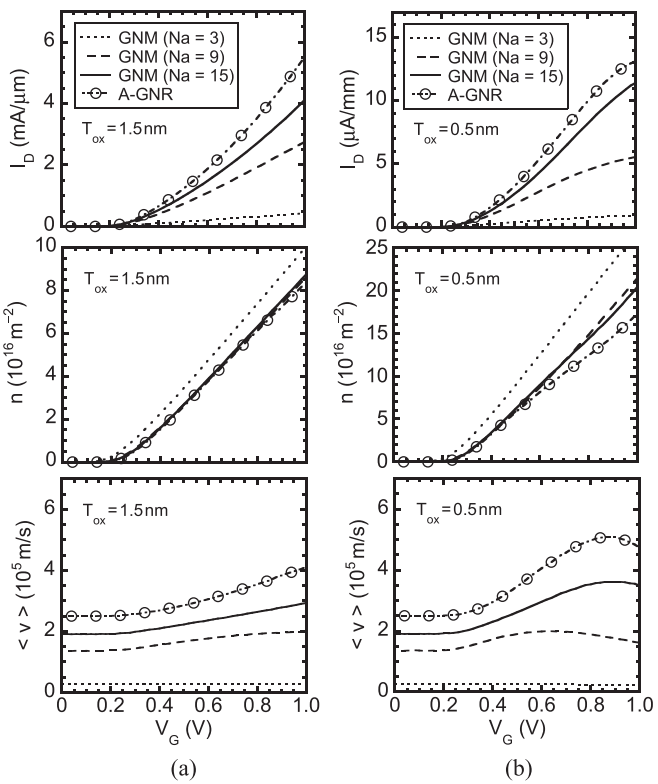

FIG. 7. Electrical characteristics computed for GNM-FETs with $N_a = 3$ (dotted lines), 9 (dashed lines), and 15 (solid lines) for T_{ox} = (a) 1.5 and (b) 0.5 nm, where N_z was fixed to be 4. Results for an A-GNR-FET with a similar band gap to the GNM with $N_a = 15$ are also plotted in the dashed-dotted lines with circles. $V_D = 0.3$ V and $I_{OFF} = 0.01$ μA/μm. Temperature is 300 K.

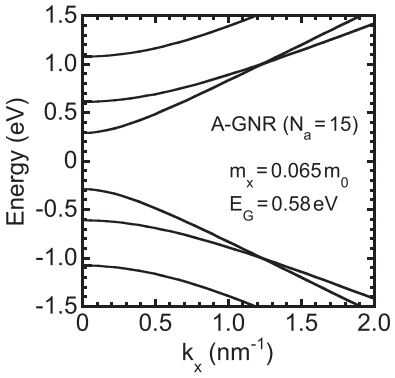

FIG. 8. Band structure of A-GNR channel used in the calculation of Fig. 7, where the number of carbon atoms in width direction is 15, and band gap 0.58 eV and effective mass 0.065 m_0.

Next, we discuss the T_{ox} dependence of the electrical characteristics. Comparing Figs. 7(a) and 7(b), the average velocity saturation and even reduction are observed for the GNMs at high gate voltages for $T_{ox} = 0.5$ nm. This is due to the fact that by reducing the gate oxide thickness, electrons begin to get populated into the flat dispersion band Z in a higher energy region of the GNMs. In Fig. 7, we also plotted the results for an A-GNR-FET with a similar band gap to that of the GNM with $N_a = 15$, in the dashed-dotted lines with circles. The band structure of the A-GNR channel is shown in Fig. 8, where the number of carbon atoms in the width direction is set as 15 and the band gap is 0.58 eV. The effective mass is calculated to be 0.065 m_0, which is smaller than 0.074 m_0 of the GNM with $N_a = 15$ by approximately 12%. The present comparison indicates that the GNM-FET with $N_a = 15$ provides the sufficiently-high drain current at less than $V_G = 1.0$ V, and even favorably compare with that of the A-GNR-FET. Although the average velocity is higher in the A-GNR-FET due to the smaller transport effective mass, the sheet electron density is found to be larger in the GNM-FETs. Accordingly, GNM-FETs have the potential ability providing high current drivability when operating at low supply voltages.

IV. CONCLUSION

We have calculated the band structures of GNMs based on the TB approach, and further estimated the electrical characteristics of GNM-FETs under the ballistic transport. As a result, we have shown that GNMs have the possibility of band structure engineering by introducing nanoholes into a graphene thin film and properly choosing the neck width. We have also demonstrated that GNM-FETs exhibit a current drive comparable to an A-GNR-FET, by controlling the neck width to exploit the superior transport properties of A-GNRs. Therefore, GNM is expected to be a promising FET channel material, providing high current drivability at low supply voltages.

ACKNOWLEDGMENTS

This work was supported by Grants-in-Aid for Scientific Research from the Japan Society for the Promotion of Science (JSPS) and the Japan Science and Technology Agency (JST)/CREST.

[1]K. S. Novoselov, A. K. Geim, S. V. Morozov, D. Jiang, Y. Zhang, S. V. Dubonos, I. V. Grigorieva, and A. A. Firsov, Science **306**, 666 (2004).
[2]T. Ohta, A. Bostwick, T. Seyller, K. Horn, and E. Rotenberg, Science **313**, 951 (2006).
[3]H. Min, B. Sahu, S. K. Banerjee, and A. H. MacDonald, Phys. Rev. B **75**, 155115 (2007).
[4]N. Harada, M. Ohfuti, and Y. Awano, Appl. Phys. Express **1**, 024002 (2008).
[5]J. B. Oostinga, H. B. Heersche, X. Liu, A. F. Morpurgo, and L. M. K. Vandersypen, Nature Mater. **7**, 151 (2008).
[6]Y. Zhang, T.-T. Tang, C. Girit, Z. Hao, M. C. Martin, A. Zettl, M. F. Crommie, Y. R. Shen, and F. Wang, Nature **459**, 820 (2009).
[7]H. Miyazaki, K. Tsukagoshi, A. Kanda, M. Otani, and S. Okada, Nano Lett. **10**, 3888 (2010).
[8]R. Sako, H. Tsuchiya, and M. Ogawa, IEEE Trans. Electron Devices **58**, 3300 (2011).
[9]H. Tsuchiya, H. Hosokawa, S. Sako, N. Hasegawa, and M. Ogawa, Jpn. J. Appl. Phys., Part 1 **51**, 055103 (2012).
[10]E. Sano and T. Otsuji, Jpn. J. Appl. Phys., Part 1 **48**, 041202 (2009).
[11]H. Hosokawa, R. Sako, H. Ando, and H. Tsuchiya, Jpn. J. Appl. Phys., Part 1 **49**, 110207 (2010).
[12]M. Fujita, K. Wakabayashi, K. Nakada, and K. Kusakabe, J. Phys. Soc. Jpn. **65**, 1920 (1996).
[13]G. Liang, N. Neophytou, D. E. Nikonov, and M. S. Lundstrom, IEEE Trans. Electron Devices **54**, 677 (2007).
[14]M. Y. Han, B. Özyilmaz, Y. Zhang, and P. Kim, Phys. Rev. Lett. **98**, 206805 (2007).
[15]X. Li, X. Wang, L. Zhang, S. Lee, and H. Dai, Science **319**, 1229 (2008).
[16]Y.-W. Son, M. L. Cohen, and S. G. Louie, Phys. Rev. Lett. **97**, 216803 (2006).
[17]J. Cai, P. Ruffieux, R. Jaafar, M. Bieri, T. Braun, S. Blankenburg, M. Muoth, A. P. Seitsonen, M. Saleh, X. Feng, K. Müllen, and R. Fasel, Nature **466**, 470 (2010).
[18]D. Gunlycke and C. T. White, Phys. Rev. B **77**, 115116 (2008).
[19]H. Tsuchiya, H. Ando, S. Sawamoto, T. Maegawa, T. Hara, H. Yao, and M. Ogawa, IEEE Trans. Electron Devices **57**, 406 (2010).
[20]R. Sako, H. Hosokawa, and H. Tsuchiya, IEEE Electron Device Lett. **32**, 6 (2011).
[21]G. Fiori and G. Iannaccone, IEEE Electron Device Lett. **28**, 760 (2007).
[22]T. Fang, A. Konar, H. Xing, and D. Jena, Phys. Rev. B **78**, 205403 (2008).
[23]Y. Yang and R. Murali, IEEE Electron Device Lett. **31**, 237 (2010).
[24]A. Yazdanpanah, M. Pourfath, M. Fathipour, H. Kosina, and S. Selberherr, IEEE Trans. Electron Devices **59**, 433 (2012).
[25]J. Bai, X. Zhong, S. Jiang, Y. Huang, and X. Duan, Nature Nanotech. **5**, 190 (2010).
[26]X. Liang, Y.-S. Jung, S. Wu, A. Ismach, D. L. Olynick, S. Cabrini, and J. Bokor, Nano Lett. **10**, 2454 (2010).
[27]T. G. Pedersen, C. Flindt, J. Pedersen, N. A. Mortensen, A.-P. Jauho, and K. Pedersen, Phys. Rev. Lett. **100**, 136804 (2008).
[28]H. Jippo, M. Ohfuchi, and C. Kaneta, Phys. Rev. B **84**, 075467 (2011).
[29]W. Liu, Z. F. Wang, Q. W. Shi, J. Yang, and F. Liu, Phys. Rev. B **80**, 233405 (2009).
[30]A. H. Castro Neto, F. Guinea, N. M. R. Peres, K. S. Novoselov, and A. K. Geim, Rev. Mod. Phys. **81**, 109 (2009).
[31]P. Zhao, J. Chauhan, and J. Guo, Nano Lett. **9**, 684 (2009).
[32]C.-H. Park, L. Yang, Y.-W. Son, M. L. Cohen, and S. G. Louie, Nature Phys. **4**, 213 (2008).
[33]A. Rahman, J. Guo, S. Datta, and M. S. Lundstrom, IEEE Trans. Electron Devices **50**, 1853 (2003).